European Journal of Pharmaceutics and Biopharmaceutics 75 (2010) 137–147

Contents lists available at ScienceDirect

European Journal of Pharmaceutics and Biopharmaceutics

journal homepage: www.elsevier.com/locate/ejpb

Research paper

Tumor targeting of functionalized lipid nanoparticles: Assessment by *in vivo* fluorescence imaging

Mathieu Goutayer [a,1,2], Sandrine Dufort [b,c,1], Véronique Josserand [b], Audrey Royère [d], Emilie Heinrich [a], Françoise Vinet [a], Jérôme Bibette [d], Jean-Luc Coll [b], Isabelle Texier [a,*]

[a] CEA, LETI-DTBS, Grenoble cedex, France
[b] INSERM U823, Institut Albert Bonniot, La Tronche, France
[c] UF Cancérologie Biologique et Biothérapie, CHU de Grenoble, La Tronche, France
[d] Laboratoire des Colloïdes et Matériaux divisés, ESPCI, Paris cedex, France

ARTICLE INFO

Article history:
Received 27 October 2009
Accepted in revised form 3 February 2010
Available online 10 February 2010

Keywords:
Lipid nanoparticles
cRGD functionalization
Fluorescence imaging
Cellular targeting
In vivo targeting
Tumor nanoparticle uptake

ABSTRACT

Lipid nanoparticles (LNP) coated by a poly(oxyethylene) polymer have been manufactured from low cost and human use-approved materials, by an easy, robust, and up-scalable process. The incorporation in the formulation of maleimide-grafted surfactants allows the functionalization of the lipid cargos by targeting ligands such as the cRGD peptide binding to $\alpha_v\beta_3$ integrin, a well-known angiogenesis biomarker. LNP are able to encapsulate efficiently lipophilic molecules such as a fluorescent dye, allowing their *in vivo* tracking using fluorescence imaging. *In vitro* study on HEK293(β3) cells over-expressing the $\alpha_v\beta_3$ integrins demonstrates the functionalization, specific targeting, and internalization of cRGD-functionalized LNP in comparison with LNP-cRAD or LNP-OH used as negative controls. Following their intravenous injection in *Nude* mice, LNP-cRGD can accumulate actively in slow-growing HEK293(β3) cancer xenografts, leading to tumor over skin fluorescence ratio of 1.53 ± 0.07 (n = 3) 24 h after injection. In another fast-growing tumor model (TS/A-pc), tumor over skin fluorescence ratio is improved (2.60 ± 0.48, n = 3), but specificity between the different LNP functionalizations is no more observed. The different results obtained for the two tumor models are discussed in terms of active cRGD targeting and/or passive nanoparticle accumulation due to the Enhanced Permeability and Retention effect.

1. Introduction

The use of effective cancer chemotherapy drugs is mainly hindered by their low aqueous solubility, which complicates their administration, and their high toxicity, necessary in regards to cancer cells but detrimental and the origin of severe side effects for healthy tissues. A wide range of pharmaceutical nanocarriers, such as polymeric or lipid nanoparticles or micelles [1–3] and even inorganic nanoparticles [4], have been screened for reducing the administrated doses and enhancing the *in vivo* accumulation of therapeutic agents into the areas to be cured. Polymeric nanomaterials are very often composed of FDA-approved biodegradable polymers, such as poly(lactic acid) (PLA), poly(glycolic acid) (PGA), and poly(ε-caprolactone) (PCL). However, their structure and therefore their synthesis process have to be tailored for each specific application. Lipid materials are more versatile and present the advantage of a lower intrinsic toxicity, because of their compositions similar or close to those of physiological lipids.

Numerous lipid nanocarriers with different structures have been studied for therapy or imaging [5–7]: micelles [8], lipoproteins [9,10], liposomes [11], micro-emulsions [12] and nanoemulsions [13,14], solid-lipid nanoparticles (SLN) [6,15,16] and nanocapsules [17]. Because of the limited size of their core, micelles cannot store high drug payload. Lipoproteins must be isolated from fresh plasma or designed from synthetic peptides [18]. Due to their phospholipid bilayer and hydrophilic cavity, liposomes display outstanding properties for the encapsulation of hydrophilic/amphiphilic therapeutic agents. However, they are not optimized for the encapsulation of high concentrations of lipophilic drugs. They are not stable enough for being stored in injection-ready formulations for long durations, and their use usually requires the reconstitution of the solution just before injection to the patient. Lipid core nanocarriers present the advantage of a higher volume reservoir for lipophilic drug encapsulation. Nanocapsules have a liquid-lipid core encapsulated within a solid

* Corresponding author. CEA, LETI-DTBS, 17 rue des Martyrs, 38054 Grenoble cedex 9, France. Tel.: +33 438 784 670; fax: +33 438 785 787.
E-mail addresses: mathieu.goutayer@gmail.com (M. Goutayer), SDufort@chu-grenoble.fr (S. Dufort), veronique.josserand@ujf-grenoble.fr (V. Josserand), Audrey.royere@espci.fr (A. Royère), emilie.heinrich@cea.fr (E. Heinrich), francoise.vinet@cea.fr (F. Vinet), Jerome.Bibette@espci.fr (J. Bibette), jean-luc.coll@ujf-grenoble.fr (J.-L. Coll), isabelle.texier-nogues@cea.fr (I. Texier).
[1] These authors contributed equally to the work.
[2] Present address: Capsum, ESPCI, 10 rue Vauquelin, 75231 Paris cedex 5, France.

0939-6411/$ - see front matter © 2010 Elsevier B.V. All rights reserved.
doi:10.1016/j.ejpb.2010.02.007

polymeric or phospholipid shell [17]. Micro-emulsions (self-assembled, thermodynamically stable) [12] and nanoemulsions (thermodynamically instable, requiring energy for their processing) [13,14] have a liquid core, whereas solid-lipid nanoparticles (SLN) have in principle a solid one [6,15,16]. However, the frontiers between the different categories of lipid particles are not so well defined. As an example, super-cooled liquid state has been observed in different SLN formulations. The solid crystalline core of SLN can present several drawbacks, such as problems of reproducibility in the particle growth, possibility of polymorphic transitions, which can induce drug expulsion during storage, and low drug incorporation capacities due to the crystalline structure [19]. Therefore, the concept of "nanostructured" lipid carriers has been introduced by Müller et al. [5]. The idea is to obtain lipid nanoparticles with a solid but not crystalline core, in order to improve the efficiency and stability of drug encapsulation.

In this manuscript, we report the design and *in vivo* bio-distribution of new lipid nanoparticles (LNP), which lipid core is composed of a mixture of oil and wax, solid at room temperature for improved stability and liquid at body temperature (≈37–40 °C melting point). The core of the LNP therefore provides a reservoir suitable for the encapsulation and controlled release of lipophilic drugs and molecules. In order to demonstrate the potential of these new nanocarriers and to assess their *in vivo* fate, whole body non-invasive fluorescence imaging (FLI) in mice is used. We have recently reported the efficient loading of a lipophilic near infrared dye, DiD, within the lipid core of the LNP and the benefits of encapsulation on the dye properties (improved fluorescence quantum yield and reduced photobleaching) [20]. FLI now allows to scan in real time the bio-distribution of near infrared dye-labeled molecules (μM payloads) in whole body live mice in a few seconds with a few millimeters resolution [21–23]. FLI is a fast, low cost, sensitive, non-ionizing, non-invasive, and easy-handled screening technique.

Using DiD-loaded nanoparticles, the bio-distribution of LNP decorated by the cRGD peptide able to target $\alpha_v\beta_3$ integrins has therefore been studied *in vivo* in two mice models using the FLI technique. The functionalization of nanocargos in order to improve their vectorization and targeting properties has been a major issue explored to improve therapy and diagnostics efficiencies in the last three decades [1–3]. $\alpha_v\beta_3$ Integrins are receptors over-expressed on the angiogenic vessels grown during tumor development [24,25]. Moreover, these membrane receptors are also expressed in 25% of human cancer cells of different types (melanoma, glioblastoma, ovarian, breast cancer) [24,25]. They therefore constitute targets of choice for favoring the specific binding and uptake in malignant cells of nanoparticles loaded with a drug or contrast agent. The well-known triad peptide sequence RGD (Arg-Gly-Asp), which recognizes the $\alpha_v\beta_3$ integrins has been identified 20 years ago [26], and its cyclic form c[-RGDfK-] designed from the peptides developed by Kessler's group provides easy conjugation to imaging and/or therapeutic moieties [24,27,28]. Grafting onto the LNP of the cRGD targeting ligand, the cRAD peptide negative control or a non-targeting –OH group is hereafter assessed by *in vitro* test on HEK293(β3) cultured cells, before the functionalized LNP are injected intravenously in two mice models, HEK293(β3) and TS/A-pc. The HEK293(β3) cell line (human embryonic kidney) has been genetically modified to strongly express $\alpha_v\beta_3$ integrins and has been successfully used as a study model for a few years [29–31]. TS/A-pc (mice mammary carcinoma cells) is another model which express naturally $\alpha_v\beta_3$ integrins [32]. Whenever injected subcutaneously in a *Nude* mouse model, TS/A-pc cells will grow faster (10 days) than HEK293(β3) cells (6 weeks) before reaching the size at which tumor imaging is performed. It is important whenever designing a new fluorescent probe or a drug delivery vector to demonstrate its potentialities in different animal models. In this study, LNP-cRGD-specific targeting is studied in comparison with negative control LNP-cRAD and non-targeted LNP-OH in the two different mice models, HEK293(β3) and TS/A-pc, which can be targeted using the same ligand, but differ in their growing process.

2. Materials and methods

2.1. Materials

Suppocire NC™ is a kind gift from Gatéfossé (France), Myrj® 53 a kind gift from Croda Uniqema (France). The thio-acetylated peptides c(RGDfK(Ac-S-CH_2CO)) (cRGD) and c(RADfK(Ac-S-CH_2CO)) (cRAD) are purchased from Asynth service B.V. (The Netherlands). DiD is purchased from Invitrogen, soybean oil, L-α-lecithin and other chemical products from Sigma–Aldrich (France). The DSPE-POE_{5000}-maleimide surfactant is prepared starting from distearyl phosphatidyl ethanolamine (DSPE, Sigma–Aldrich) and NHS-POE_{5000}-maleimide (NHS = N-succinimidyl ester, POE = poly(ethyleneoxide), Nektar, USA). To 25 mg of distearyl phosphatidyl ethanolamine (DSPE) dissolved in 1 mL anhydrous dichloromethane are added 100 mg of NHS-POE_{5000}-maleimide and 5 μL of triethylamine. The advancement of the reaction is controlled by thin layer chromatography. After 2 h stirring under argon, the solvent is evaporated under reduced pressure and the product dissolved in dichloromethane to yield a 2 mL solution that will be used directly in the functionalized formulations.

2.2. Preparation of DiD-loaded LNP

For preparation of a 2 mL dispersion batch of non-functionalized LNP, 150 mg of Suppocire® NC, 50 mg of soy bean oil, 138 mg of L-α lecithin, and 800 nmol of DiD (766 μg) are dissolved in 1 mL of dichloromethane and mixed at 45 °C. After homogenization, the organic solvent is evaporated under reduced pressure and the lipid phase is crudely mixed with the continuous phase composed of 228 mg of Mirj® 53, 50 mg of glycerol and NaCl 154 mM (1.38 mL). For the functionalized formulations, the compositions of both the dispersed and continuous phases are slightly modified. In this case, for the preparation of a 2 mL dispersion batch of LNP-maleimide, 150 mg of Suppocire® NC, 50 mg of soy bean oil, 138 mg of L-α lecithin, 49 mg of DSPE-POE_{5000}-maleimide (880 μL of the solution prepared as described earlier), and 800 nmol of DiD (766 μg) are dissolved in 0.5 mL of dichloromethane and mixed at 45 °C. After homogenisation, the organic solvent is evaporated under reduced pressure, and the lipid phase is crudely mixed with the continuous phase composed of 207 mg of Mirj® 53, 50 mg of glycerol, and 1.36 mL of buffer (HEPES 0.05 M, EDTA 0.01 M, pH 7.4). After crude mixing at 45 °C of the dispersed and continuous phases, emulsification is carried out by sonication (AV505 Ultrasonic processor, Sonics, USA) performed at 40 °C for 5 min. A translucent blue solution is obtained, which is then purified by overnight extensive dialysis carried out at room temperature against 1000 times its volume in the appropriate aqueous buffer (NaCl for LNP, HEPES/EDTA buffer for LNP-maleimide) using a 12–14,000 Da MW cut-off membrane (ZelluTrans, Roth, France). When further functionalization is carried out, 600 μL of crude LNP-maleimide are diluted in 400 μL of grafting buffer (HEPES 0.05 M, EDTA 0.01 M, pH 7.4). In an aqueous 40 mM tris(2-carboxyethyl)phosphine solution, 3.75 μmol of the cRGD or cRAD peptides are dissolved and stirred for 30 min before being added to the LNP-maleimide solution. After stirring for 2 h in dark at ambient temperature, 7.5 μmol of 2-mercapto-ethanol are added to the dispersion in order to quench the surface maleimide groups that would not have reacted. After 30 min stirring in dark at room temperature, extensive dialysis against NaCl 154 mM is performed

using a 12–14,000 Da MW cut-off membrane (ZelluTrans) to yield purified LNP-cRGD or LNP-cRAD. To obtain LNP-OH, only the quenching step with the addition of 2-mercaptoethanol and the further purification are performed. Finally, all the LNP dispersions are filtered through a 0.22-μm Millipore membrane for sterilization before characterization and/or injection.

2.3. Physico-chemical characterizations

Cryo-TEM (Transmission Electron Microscopy) analysis is performed using a MET microscope (JEOL 2100HC) with a LaB_6 electron source operating at 200 kV. The sample is deposited onto a holey carbon grid, blotted to remove excess liquid, and frozen by plunging rapidly into liquid ethane (−185 °C). The hydrodynamic diameter and zeta potential of the lipid nanoparticles are measured with a Malvern Zeta Sizer Nano instrument (NanoZS, Malvern, UK) in 0.1× PBS buffer. The absorbance and fluorescence measurements are performed, respectively, using a Cary 300 Scan (Varian, Massy, France) UV–visible spectrophotometer and a Perkin Elmer LS50B fluorimeter (Perkin, Coutaboeuf, France). The absolute fluorescence quantum yields QY) are calculated by comparison with a standard of known QY (Nile blue perchlorate in ethanol (QY = 0.27) [33] at 600 nm excitation, as previously described [20].

2.4. Cell lines and culture conditions

HEK293(β3), stable transfectants of human β3 from the human embryonic kidney cell line (kindly provided by J.-F. Gourvest, Aventis, France), are cultured as previously described in DMEM supplemented with 1% glutamine, 10% fetal bovine serum (FBS), 50 units/mL penicillin, 50 μg/mL streptomycin, and 700 μg/mL Geneticin (G418 sulfate, Gibco, Paisley, UK) [29,30]. TS/A-pc are mouse mammary cancer cells cultured in RPMI 1640 supplemented with 1% glutamine, 10% fetal bovine serum (FBS), 25 nM 2-mercaptoethanol, 50 units/mL penicillin, and 50 μg/mL streptomycin [32]. All cell lines are cultured at 37 °C in a humidified 95% air/5% CO_2 atmosphere. All the cells used here are integrin $\alpha_v\beta_3$-positive [29,30,32].

2.5. Fluorescence microscopy analysis of functionalized LNP incubated in the presence of HEK293(β3) cells

HEK293(β3) cells – 10^6 per well – are grown on coverslips overnight at 37 °C, rinsed once with PBS, then with PBS containing 1 mM $CaCl_2$ and 1 mM $MgCl_2$. They are then incubated for 15 min at 4 °C (binding analysis) or 1 h at 37 °C (internalization analysis) in the presence of either LNP-cRGD, LNP-cRAD, or LNP-OH at a concentration of 0.2 μM DiD and 141 μg/mL of total lipids. They are subsequently rinsed with PBS Ca^{2+}/Mg^{2+} (1 mM) and fixed (10 min with 0.5% paraformaldehyde). Nuclei are labeled with Hoechst 33342 (Sigma Aldrich, St. Quentin Fallavier, France) (5 μM) during 10 min. After being rinsed with PBS, coverslips are mounted in Mowiol. Fluorescence microscopy is performed on Axiophot (Carl Zeiss, Jena, Germany). The same experiment is performed also in serum conditions (culture medium with 10% of fetal bovine serum).

2.6. Flow cytometry analysis of functionalized LNP incubated in the presence of HEK293(β3) cells

For binding analysis, adherent cells are resuspended with trypsin, washed once with cold PBS, and another time with PBS containing 1 mM $CaCl_2$ and 1 mM $MgCl_2$. One million cells in a final volume of 200 μL are resuspended in LNP suspension (0.2 μM DiD, 141 μg/mL total lipids) in PBS Ca^{2+}/Mg^{2+} (1 mM) and incubated 15 min at 4 °C. LNP solutions are removed and pellets carefully rinsed twice with PBS Ca^{2+}/Mg^{2+} (1 mM) at 4 °C. Cells are then rapidly analyzed by flow cytometry (FACS Arial, Becton Dickinson, France). The results are reported as DiD fluorescence (FL4) histogram counts. For internalization analysis, the same experiment is performed with reagents at 37 °C, and the LNP suspensions are incubated 1 h at 37 °C.

2.7. In vivo fluorescence imaging

Female NMRI *Nude* mice (6–8 weeks old, JANVIER, Le Genest Saint Isle, France) receive a sub-cutaneous xenograft of HEK293(β3) cells (20×10^6 per mouse) or TS/A-pc cells (10×10^6 per mouse). After tumor growth, mice ($n = 3$ for each group) are anesthetized (isoflurane/oxygen 4%/3.5% for induction and 2% thereafter) and are injected intravenously in the tail vein with 200 μL of LNP suspension (10 nmol DiD, 7.1 mg of total lipids), then they are illuminated by 660-nm light-emitting diodes equipped with interference filters. Fluorescence images as well as black and white pictures are acquired by a back-thinned CCD camera at −80 °C (ORCAII-BT-512G, Hamamatsu, Massy, France) fitted with high pass filter RG 9 (Schott, Jena, Germany) [29,30,32,34,35]. All the animal experiments are performed in agreement with the EEC guidelines and the "Principles of Laboratory Animal Care" (NIH Publication No. 86-23, revised 1985). After imaging, the mice are killed and dissected for imaging organs. Image display and analysis are performed using the Wasabi software (Hamamatsu, Massy, France). Semi-quantitative data are obtained from the fluorescence images by drawing regions of interest (ROI) on the subcutaneous tumors. Similar ROI are also positioned on the skin of the back of each mouse, in a similar position to the tumor, but on the other side of the mouse. The number of photons collected into each ROI is then used to calculate the tumor/skin ratios. The results of organ fluorescence quantifications are expressed as a number of relative light units (RLU) per pixel.

2.8. Statistical analysis

All the data are given as mean ± standard deviation (SD) of three independent measurements. Statistical analysis is performed using two-tailed nonparametric Mann–Whitney *t*-test. Statistical significance is assigned for values of $p < 0.05$.

3. Results

3.1. Design and characterization of lipid nanoparticles

Numerous active pharmaceutical ingredients are efficient *in vitro* at the cellular level, but cannot be used *in vivo* because of their high hydrophobicity that precludes their direct administration. Nanoparticles with a lipid core constitute ideal cargos for the vectorization of high payloads of these lipophilic compounds. We here report the design of new lipid nanoparticles (LNP) based on the use of low cost, Generally Recognized As Safe (GRAS) ingredients, such as oil, lecithine, and poly(oxyethylene) (POE) surfactants. LNP are manufactured by sonication, a versatile and upscalable process. The lipid core is composed of a mixture of oil and wax, solid at ambient temperature, but melting at body temperature (≈37–40 °C), which should favor both the stability of the colloidal suspension during storage and controlled drug delivery *in vivo*. LNP can moreover be efficiently loaded by a lipophilic dye, DiD, in order to allow their *in vitro* and *in vivo* tracking [20].

In practice, LNP are manufactured following the steps described in Scheme 1. The oily phase composed of lipids with very low aqueous solubility (soybean oil and Suppocire® wax), phospholipids (lecithine), and the lipophilic molecule to be vectorized (in this

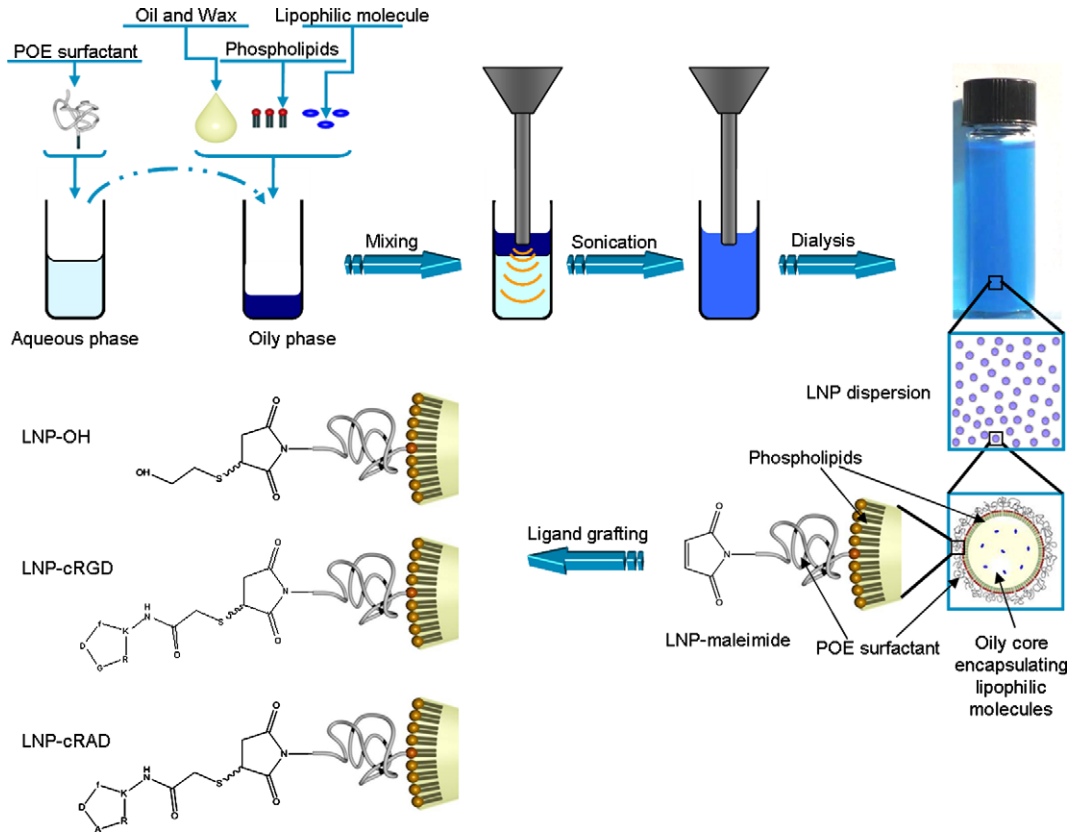

Scheme 1. Manufacturing process and structure of functionalized lipid nanoparticles. The aqueous phase containing the POE surfactant (Myrj® 53) is mixed with the lipid phase, constituted by oil and wax, phospholipids, the lipophilic dye (DiD), and eventually the DSPE-POE-maleimide surfactant. After mixing and sonication, the LNP dispersion is dialyzed against NaCl 154 mM buffer. The lipid droplets are 35 nm diameter, which leads to a translucent colloidal dispersion. The maleimide groups of the functionalized LNP particles can further be derivatized by thiol-bearing molecules such as 2-mercaptoethanol or peptides c(RGDfK(Ac-SH)) and c(RADfK(Ac-SH)), leading, respectively, to LNP-OH, LNP-cRGD, or LNP-cRAD particles. (For interpretation of the references to colour in this figure legend, the reader is referred to the web version of this article.)

work the DiD dye) is mixed with the continuous phase composed of physiological buffer, poly(oxyethylene) surfactant (Mirj® 53, ≈50 oxyethylene motifs), and glycerol. The role of glycerol is to facilitate the emulsification step, which is carried out at 45 °C by 5 min ultrasonication (Scheme 1). A dispersion of lipid droplets encapsulating the DiD dye and stabilized in surface by the mixture of phospholipids (lecithine) and POE surfactants (Mirj® 53) is thus obtained. The typical droplet size as measured by dynamic light scattering in NaCl 154 mM is 35 ± 2 nm, with a polydispersity index of 0.17 ± 0.02 (Table 1). The zeta potential of the particles is −5 ± 2 mV, demonstrating that their surface can be considered as neutral.

In order to be able to graft targeting ligands, such as the cRGD peptide, onto the LNP surface, 9.2% of Mirj® 53 is replaced by DSPE-POE_{5000}-maleimide (DSPE = distearyl phosphatidyl ethanolamine), while keeping constant the total quantity of POE surfactants. DSPE-POE_{5000}-maleimide is a surfactant which poly(oxyethylene) chain contains ≈110 oxyethylene motifs (longer than the ≈50 oxyethylene motifs of the Mirj® 53 surfactant) and to which is grafted a maleimide coupling group at the hydrophilic extremity. After dialysis purification of the LNP-maleimide particles, classical thiol-maleimide coupling is performed in the presence of 2-mercaptoethanol, cRGD-SH, or cRAD-SH, in order to lead, respectively, to non-targeting LNP-OH, targeting LNP-cRGD, or negative control LNP-cRAD (Scheme 1).

Table 1
Physico-chemical properties of functionalized lipid nanoparticles.

Particles	Hydrodynamic diameter (nm)[a]	Polydispersity index[a]	Zeta potential (mV)[a]	QY[b]
LNP	35 ± 2	0.17 ± 0.02	−5 ± 2	0.38
LNP-maleimide	34 ± 2	0.21 ± 0.02	–	0.39
LNP-OH	35 ± 2	0.22 ± 0.02	−3 ± 2	0.39
LNP-cRGD	35 ± 2	0.16 ± 0.03	−3 ± 2	0.40
LNP-cRAD	35 ± 2	0.15 ± 0.03	−3 ± 2	0.40

[a] The error bar represents the standard deviation for at least three measurements per batch on two different batches.
[b] The fluorescence quantum yields (QY) of DiD-loaded LNP are recorded at 600 nm excitation; the estimated error on the values is 5%.

The functionalization of the LNP does not modify dramatically their physico-chemical properties, as reported in Table 1 and Fig. 1. The introduction of the DSPE-POE_{5000}-maleimide surfactants in the particle shell that already contains Myrj® 53 does not increase the particle hydrodynamic diameter (35 ± 2 nm), probably because the long polymer chains are in a coiled configuration. The polydispersity index is slightly increased for LNP-maleimide and LNP-OH (Table 1), which could be indicative of a lower stability for these colloidal suspensions. Interestingly, the shape of the particles as observed by cryo-transmission electronic microscopy (cryo-TEM) is not spherical but rather the lipid droplets appear oblong (Fig. 1). Similar non-spherical shapes have been reported for SLN and other lipid nanoparticles when observed by this technique [15]. The introduction of the functional groups does not affect the zeta potential either, which remains close to neutrality (Table 1): the introduced peptides or hydroxyl functions are globally neutral at pH 7–8. Moreover, the encapsulation of the DiD dye is not affected by the surface functionalization, and the fluorophore displays similar optical properties once loaded within the LNP core

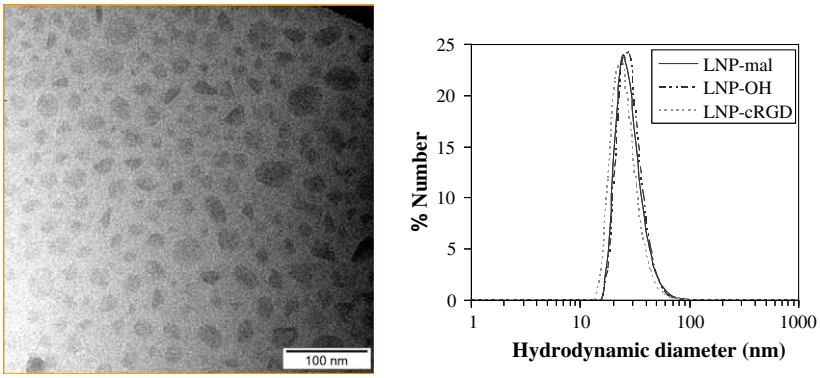

Fig. 1. Structural characterization of lipid nanoparticles. Cryo-TEM microscopy photograph (left) evidences non-spherical particles, probably with an oblong shape, and of characteristic dimension ≈35 nm. Diffusion light scattering measurements (right) in dilute PBS buffer (0.1×) evidences one population of particles with an hydrodynamic diameter of 35 nm, whatever the functional group on the surface (maleimide, –OH, cRGD). (For interpretation of the references to colour in this figure legend, the reader is referred to the web version of this article.)

(absorption and emission maximum, respectively, at 646 and 668 nm, similar fluorescence quantum yield, Table 1).

The maximum number of targeting peptides (cRGD or cRAD) grafted onto the nanoparticle surface can be estimated by the

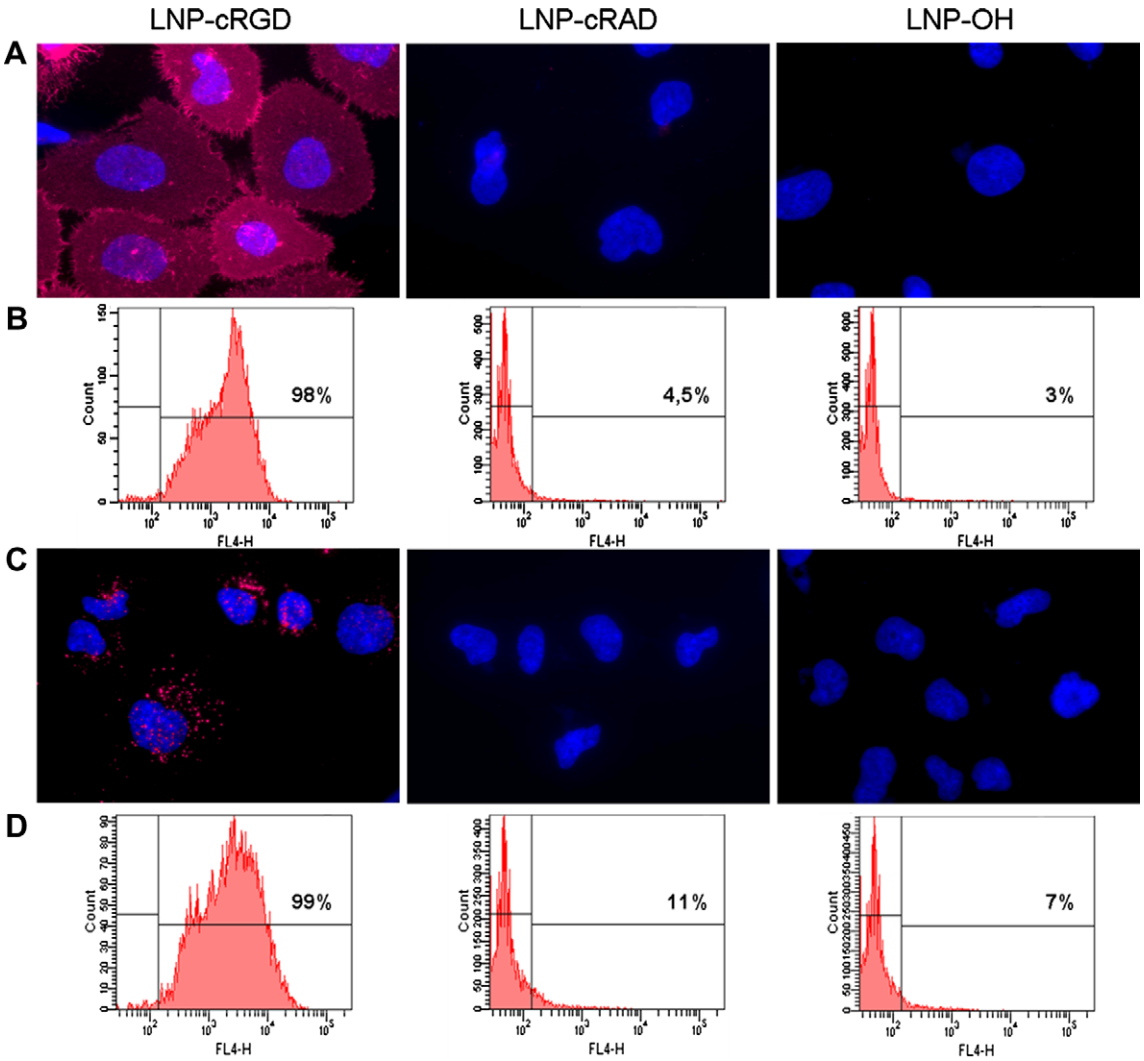

Fig. 2. *In vitro* test of LNP-cRGD, LNP-cRAD, LNP-OH (0.2 μM DiD, 141 μg/mL of lipids) in the presence of HEK293(β3) cells after 15 min incubation at 4 °C (A and B) or 1 h at 37 °C (C and D) in the presence of 10% fetal bovine serum. Fluorescence microscopy images (A and C) and flow cytometry analysis (B and D) evidence the specific LNP-cRGD (red) binding (A and B) and internalization (C and D), in comparison with negative control LNP-cRAD and non-functionalized LNP-OH. The cell nuclei are labeled in blue (Hoechst) on the fluorescence microscopy photographs (A and C). The figures on the flow cytometry plots (B and D) represent the percentages of labeled cells. (For interpretation of the references to colour in this figure legend, the reader is referred to the web version of this article.)

rough calculation of the number of maleimide groups incorporated in the LNP surface during the emulsification process. Assuming all the DSPE-POE_{5000}-maleimide surfactants are incorporated in the LNP surface and for an estimated concentration of 1.2×10^{16} particles/mL (35 nm diameter particles) [20], a maximum number of 208 maleimide groups and therefore cRGD or cRAD peptides per particle is obtained (roughly 1 function par 20 nm^2 on the particle surface, for a total of 3850 nm^2 per particle).

As already observed for DiD-loaded LNP [20], the LNP-cRGD, LNP-cRAD, and LNP-OH, functionalized particles display a high colloidal stability when dispersed in NaCl 154 mM: no modification of either the particle size or zeta potential have been observed for 1 month storage at 4 °C in dark. Therefore, functionalized LNP can be confidently tested for *in vivo* and *in vitro* applications.

3.2. In vitro targeting and internalization of LNP

Functionalization of the LNP by the cRGD targeting ligand is first checked *in vitro*. Targeted LNP-cRGD, negative control LNP-cRAD, and non-functionalized LNP-OH are incubated in the presence of HEK293(β3) cells. The HEK293(β3) cell line has been genetically modified to over-express $\alpha_v\beta_3$ integrins. Fig. 2 summarizes the results obtained both by flow cytometry and fluorescence microscopy after incubation of 6.0×10^{12} particles/mL (0.2 μM of DiD dye, 141 μg/mL of total lipids) with HEK293(β3) cells in the presence of 10% fetal bovine serum. The incubation at 4 °C is suitable for studying specific targeting (Fig. 2A and B), whereas incubation at 37 °C allows particle internalization (Fig. 2C and D). Both flow cytometry and fluorescence microscopy evidence specific HEK293(β3) targeting of cRGD-functionalized LNP, in comparison with LNP-cRAD and non-functionalized LNP-OH after 15 min of incubation at 4 °C. The specific interaction of HEK293(β3) cells with LNP-cRGD leads to the internalization of the particles with an endosome-like pattern after 1-h incubation at 37 °C, as evidenced by fluorescence microscopy (Fig. 2C). Pre-saturation of the HEK293(β3) cells with 10 μM free cRGD for 5 min before LNP-cRGD incubation inhibits cell fluorescence labeling (results not shown). The results are similar whatever absence or presence of 10% fetal bovine serum in cell culture medium, indicating that non-specific interactions should not occur between the LNP and serum proteins. The dense poly(oxyethylene) coating of the nanoparticles seems to be efficient in preventing protein binding.

3.3. In vivo targeting of LNP

The *in vivo* behavior of LNP is then assessed following their intravenous injection in the tail vein of *Nude* mice bearing HEK293(β3) xenografts in their right flank. The fluorescence images obtained at different times after LNP injection (50 μM DiD, 35 mg of total lipids) are presented in Fig. 3. Similarly to the

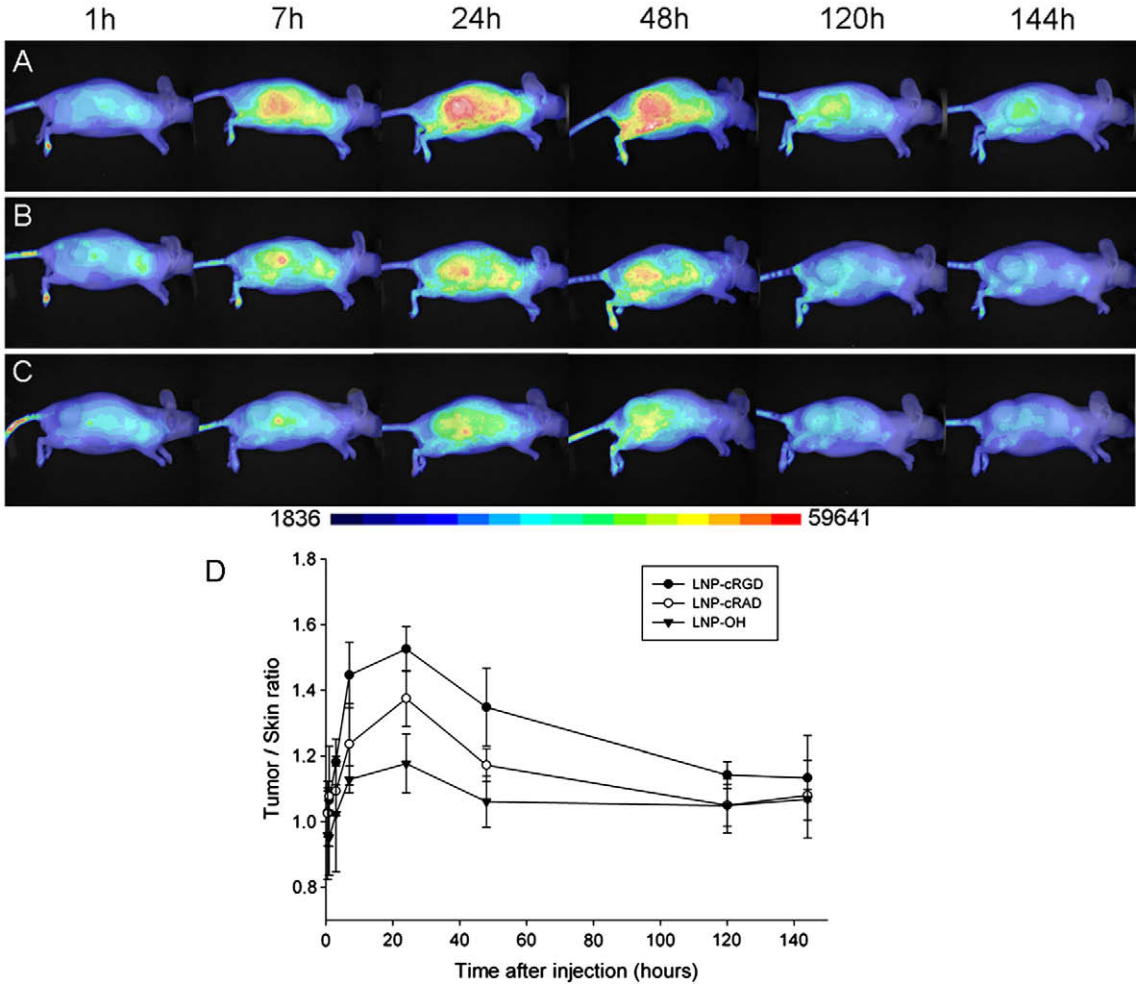

Fig. 3. *In vivo* injection of LNP-cRGD (A), LNP-cRAD (B), or LNP-OH (C) (10 nmol DiD, 7.1 mg of lipids dispersed in 200 μL) in HEK293(β3) xenografted *Nude* mice. Fluorescence images (200 ms integration time, color scale with contrast fixed between 1836 and 59,641) are recorded at different times after injection and superimposed to visible light images (in white and black) (A–C). Tumor over skin fluorescence ratio (D) is calculated by drawing regions of interest (ROI). (For interpretation of the references to colour in this figure legend, the reader is referred to the web version of this article.)

results obtained on cell cultures *in vitro*, an active accumulation of cRGD-targeted particles is observed in the tumor area, in comparison with LNP-OH. The maximum of the fluorescence signal is achieved 24 h after injection, and the tumor is still clearly delimitated 48 h after injection. Further quantification of the tumor over skin ratio 24 h after injection sustains LNP-cRGD targeting ($T/S = 1.53 \pm 0.07$, $n = 3$) in comparison with non-functionalized LNP-OH ($T/S = 1.18 \pm 0.09$, $n = 3$). Surprisingly, a slight effect of the cRAD peptide functionalization ($T/S = 1.37 \pm 0.09$, $n = 3$) is observed *in vivo* (Fig. 3), which is far less pronounced *in vitro* on the percentage of LNP-cRAD binding and internalization (Fig. 2). However, the tumor over skin contrasts overall remain poor in the HEK293(β3) tumor model.

Another tumor model is therefore tested *in vivo*. The TS/A-pc model is issued from a mouse mammary cancer cell line, known to express low levels of $\alpha_v\beta_3$ integrins on the cell membrane. However, because of their murine origin, TS/A-pc tumors are growing much faster than the human HEK293(β3) xenografts (10 days for TS/A-pc, 6 weeks for HEK293(β3)). Fig. 4 presents the results obtained *in vivo* after injection of targeting LNP-cRGD, negative control LNP-cRAD, and non-functionalized LNP-OH (50 μM DiD, 35 mg of total lipids) in *Nude* mice bearing TS/A-pc tumors. As evidenced

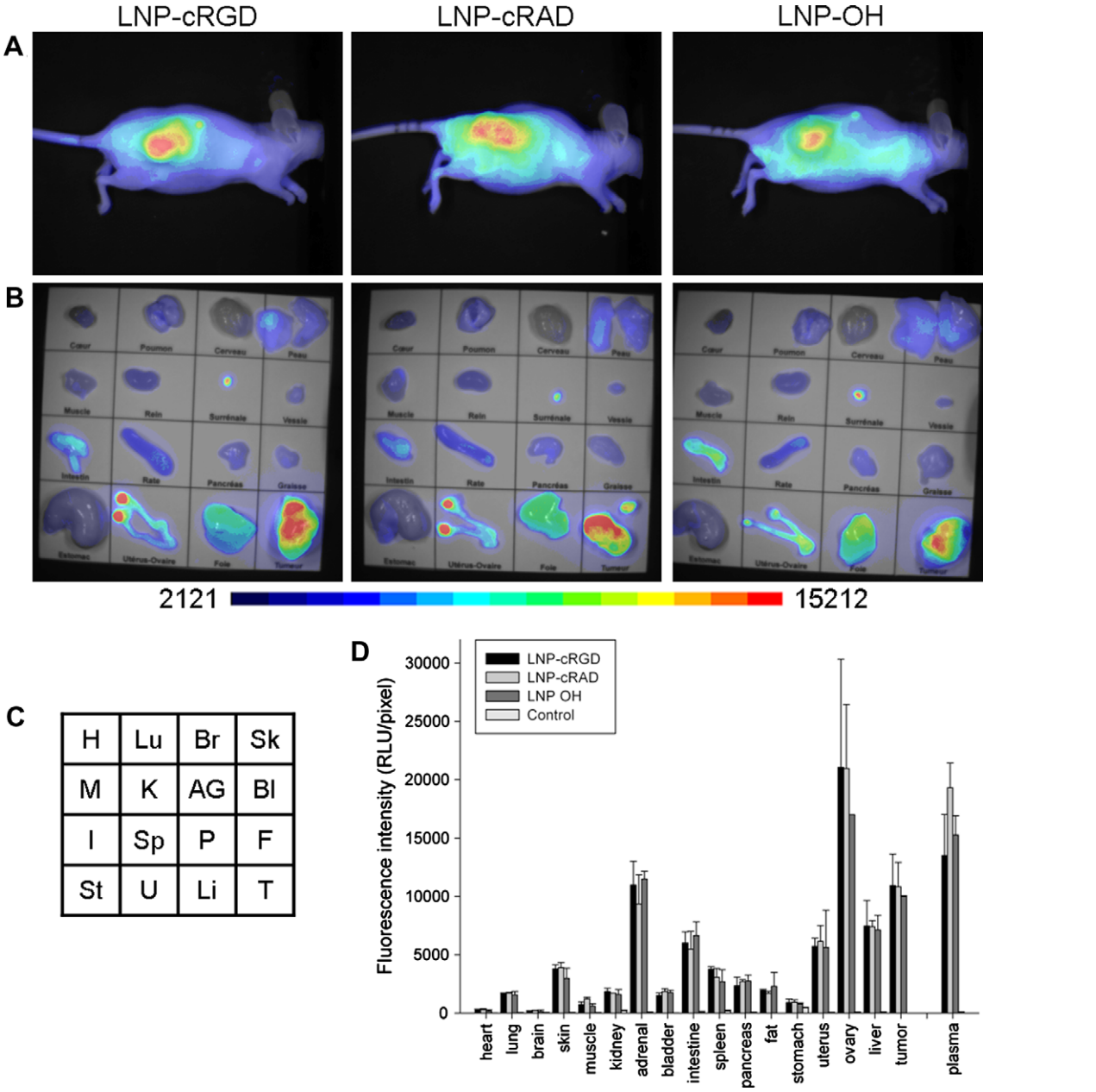

Fig. 4. *In vivo* injection of LNP-cRGD, LNP-cRAD, or LNP-OH (10 nmol DiD, 7.1 mg of lipids dispersed in 200 μL) in *Nude* mice carrying sub-cutaneous TS/A-pc tumors. (A) Fluorescence images obtained 24 h after injection evidence important accumulation of all the particles in the tumor area. Fluorescence images (20 ms integration time, color scale with contrast fixed between 2121 and 15,212) are superimposed to visible light images (in white and black). (B) Accumulation of all types of particles in tumor is confirmed by fluorescence images (20 ms integration time, color scale with contrast fixed between 2121 and 15,212, superimposed to visible light images) recorded after organ dissection (24 h after injection). The grid indicating the order of the organs is in (C). H: heart; Lu: lungs; Br: brain; Sk: skin; M: muscle; K: kidneys; AG: adrenal gland; Bl: bladder; I: intestine; Sp: spleen; P: pancreas; F: fat; St: stomach; U: uterus–ovaries; Li: liver; T: tumor. (D) Quantification of the fluorescence signal of the different organs after dissection (24 h after injection). Fluorescence is expressed in relative light unit per pixel (RLU/pix). Controls are non-injected mice. (For interpretation of the references to colour in this figure legend, the reader is referred to the web version of this article.)

by the fluorescence images 24 h after injection, contrarily to the HEK293(β3) tumors for which small active targeting of LNP-cRGD is achieved, accumulation of LNP in the TS/A-pc tumors is obtained whatever the particle coating (cRGD, cRAD, –OH) (Fig. 4A). This is also evidenced by the tumor over skin fluorescence ratio 24 h after injection: 2.60 ± 0.48 for LNP-cRGD (n = 3), 2.40 ± 0.13 for LNP-cRAD (n = 3), 2.61 ± 0.21 for LNP-OH (n = 3). Observation of the organs 24 h after injection and animal dissection confirms a similar tumor accumulation for the three coatings (Fig. 4B–D). The whole body and organ fluorescence images evidence a rather homogeneous bio-distribution of the fluorescence signal in areas different from the tumor and the brain. The brain is not labeled, indicating that the LNP cannot cross the Blood Brain Barrier. A few organs appear more fluorescently labeled: uterus/ovaries, adrenals, liver, and intestine. The intestine fluorescence signal cannot be attributed to auto-fluorescence from the food but is significantly related to a partial elimination of the LNP (Fig. 4D). The mouse plasma also displays important fluorescence levels 24 h after injection (Fig. 4D), which could be indicative of a long circulation time of the particles in blood.

4. Discussion

4.1. Specifications for efficient particle targeting

Nanocarriers dedicated to drug or contrast agent targeting and delivery *in vivo* (animal and ultimately human applications) should fulfill several specifications. First of all, these nanocarriers should of course display no toxicity at the administrated doses. It has to be kept in mind from the design of clinical grade particles that pharmaceutical approval will be necessary. Second, they should display prolonged circulation in blood in order to accumulate progressively in the diseased tissues, and ultimately reach specific delivery only in targeted cells [1,36].

Achieving prolonged circulation in blood implies several constraints on the physico-chemical parameters of the nanocarriers. First, the nanometer size (<100 nm) and second, colloidal stability (no risk of *in vivo* particle aggregation) are of tremendous importance for ensuring no risk of embolism and for potentially achieving targeted cell internalization. Moreover, the nanometer size has been demonstrated to favor passive accumulation of nanoparticles in tumors [37]. This process is accounted for by the increased porosity in the tumor vasculature, along with the low lymphatic drainage of cancer tissues, in comparison with the healthy ones (Enhanced Permeability and Retention (EPR) effect) [37]. Even if fenestrations of the vasculature at the tumor sites strongly depend on the cancer models [38], 20–100 nm range often appears as an optimal diameter for an efficient extravasation and retention of the nanoparticles from capillaries to the tumor interstitial tissues [39]. Particle charge constitutes the third key physico-chemical parameter to control the nanovector bio-distribution. Positively charged nanocarriers are known to be very efficiently stocked in the liver as soon as they are injected [40]. Coating of the particles by poly(oxyethylene) polymers has been a well-described strategy to limit opsonin binding and therefore rapid uptake of nanoparticles by the RES (Rethiculo-Endothelial System) organs, such as liver, spleen, and bone marrow [1,2,41–43]. Mastering all these physico-chemical parameters (size, stability, surface charge, and coating) is therefore of tremendous importance for *in vivo* applications of nanovectors.

4.2. Achieving in vivo specifications with LNP

The idea that long-lasting blood circulation will lead to a better tumor accumulation and targeting for oncology applications has driven the LNP design. The lipid nanoparticles described in this work are composed of vegetable oil and wax containing long chain triglycerides (LNP core), C_{16}–C_{18} phosphatidylcholine (lecithine phospholipids), and poly(oxyethylene)-based surfactants. All these products are already approved by the FDA for human use. The similarity of structures of the LNP ingredients and naturally encountered lipids and phospholipids should ensure a good biocompatibility and metabolization of the LNP nanocarriers (further biocompatibility and cellular toxicity studies are in progress). Moreover, long chain triglycerides (LNP core), C_{16}–C_{18} phosphatidylcholine (lecithine phospholipids, LNP shell), and poly(oxyethylene)-based surfactants (LNP shell) are ingredients known for promoting slow elimination from the blood circulation when used in emulsion formulations [16]. In addition to a suitable ingredient choice, new manufacturing process has to be used in order to achieve small particle size with high colloidal stability, and therefore long blood circulation time. Lipid nanovectors have presently diameters classically around 70–200 nm, and few formulations below 50 nm have been described [6,15,19,44]. The use of very high surfactant concentrations should ensure a small particle size while maintaining their colloidal stability. Neutral surfactants are chosen in order to achieve a near-neutrality surface of the nanocargos: (i) phospholipids (soybean lecithin) and (ii) poly(oxyethylene)-based surfactants known to improve the stealth character of nanocarriers because they reduce opsonin binding and particle macrophage uptake [1,2,41–43]. Several processes have been described for the preparation of nanometric emulsions and SLN: hot or cold homogenization, solvent emulsification/evaporation, and dilution of micro-emulsions. These methods classically rely on the solubilization of the surfactants in the aqueous phase or the use of organic solvents [6,15,19,44]. In this work, in order to be able to increase the phospholipid ratio in the LNP formulation (up to 6.9% w/w phospholipids for 10% w/w total lipids) and therefore achieve smaller nanoparticle size, lecithin is introduced in the oily phase, thanks to the solubilizing power of the mixture of soybean oil and wax. In order to obtain a dense poly(oxyethylene) coating on the particle surface, very high content of stearate-POE_{2000} (Myrj® 53, 11.4% w/w for 10% w/w total lipids) is used. Emulsification is achieved using the sonication technique. Different emulsification processes have been described for the production of nanoemulsions. Low-energy processes, such as PIT (Phase Inverse Temperature) [17,44] or Catastrophic Phase Inversion (CPI) [45,46] are advantageous for the encapsulation of fragile drugs and macromolecules but are highly dependent on the formulation composition [44]. Moreover, the introduction of modified phospholipids for the surface functionalization of the nanocarriers by targeting ligands is rather difficult in these conditions. High energy methods encompass mainly high pressure homogenization and sonication [47]. One advantage of sonication, however not widely used, is the fact that low to large volumes of highly viscous solutions can be easily processed. Moreover, as a high energy method, it allows the manufacturing of a wide range of formulations, and the incorporation in the composition of maleimide modified surfactants for further grafting of targeting ligands on the nanoparticles does not modify the processing. Thanks to this new manufacturing process, particle size of 35 nm diameter can be easily achieved (Table 1, Fig. 1). Moreover, the colloidal stability of the formulation is more than 1 year for LNP [20] and at least 1 month for LNP-cRGD, LNP-cRAD, and LNP-OH kept at 4 °C. This very good colloidal stability should be accounted for, at least partly, by the very dense POE coating that prevents particle coalescence. The use of non-ionic POE and zwitterionic phospholipid (lecithine) surfactants ensures a particle charge as measured by zeta potential in solution close to neutrality ($\zeta = -5 \pm 2$ mV). This should also limit opsonin binding whenever particles are in blood circulation. Therefore, LNP seem to fulfill the different chemico-physical constraints

associated to *in vivo* applications of nanoparticles: small size, high colloidal stability, neutral charge, and POE coating. In addition, these sub-100-nm nanocarriers can be sterilized using micro-filtration, a process easier to manipulate than thermal or X-ray treatments, which can destabilize the lipid nanoparticles [15,19].

4.3. In vivo bio-distribution of LNP

Indeed, the small size and the POE coating of LNP seem to limit protein adsorption onto the nanoparticle surface. No effect of serum addition is observed on the specific targeting and internalization of LNP-cRGD assessed *in vitro* while incubation in the presence of HEK293(β3) cells (Fig. 2). The functionalized LNP seem to have a relatively long blood half life since all the organs (except brain) are able to be fluorescently labeled at similar levels, and since the fluorescence signal is clearly evidenced in plasma 24 h after injection (Fig. 4). It should be underlined here that fluorescence imaging is still not an absolutely quantitative method to assess bio-distribution, mainly because the different tissues (blood, plasma, organs) absorb and diffuse visible light in different manners. However, it is possible to make relative comparisons for a same organ between different particles and a non-injected animal and to drive conclusions on the fluorescence evolution over time. Another point is that fluorescence imaging allows the *in vivo* tracking of the fluorescent dye, but not truly the nanovector it is loaded into, and which might dissociate *in vivo*. The encapsulation stability of the DiD dye in the LNP core has been demonstrated to be superior to 1 year at room temperature on the laboratory shelf [20]. A very stable fluorescence signal (less than 30% decay in 48 h at 37 °C) is observed when DiD-loaded LNP dispersions are incubated in human plasma or whole blood *in vitro* (data not shown). The fluorescence signal cannot come from free DiD dye in solution, since this dye is not fluorescent in aqueous medium [20]. Therefore, the stability of the fluorescence signal is indicative either of leakage of the dye from the LNP, but followed by its adsorption on plasma proteins, or indicative of the stability of the dye encapsulation within the particle core while in plasma. Combined with the fact that a high density POE coating is present on the surface of the particle, which should prevent protein binding (no effect of calf serum proteins has been observed in *in vitro* binding study, see Section 3.2), and the fact that the lipid dye should have a very good affinity for the particle lipid core, we believe that the particle's integrity is therefore probably maintained *in vitro* in plasma and blood for a few hours at least. *In vivo*, the particle fate can of course be very different. The hydrophilic counterpart of the DiD dye, Cy5, has been shown to be readily eliminated by the kidneys when injected free *in vivo* (no similar test can be carried out with the DiD dye because of its low water solubility) [35]. All these points could indicate that the DiD dye remains loaded within the LNP core for at least a few hours while in blood circulation and that LNP DiD-loading really allows the *in vivo* tracking of the functionalized nanovectors. Further pharmacokinetics experiments, particularly using radiolabeling to allow a "true" quantitative bio-distribution, are currently planned to check this hypothesis. Assuming that the fluorescence signal reflects the LNP bio-distribution, the nanovectors seem to distribute quite uniformly in the body and have a long blood circulation time, whatever their functionalization (Figs. 3 and 4). Thorough data analysis shows that tumor is the most fluorescent tissue along with uterus/ovaries and adrenal glands. Uterus/ovaries [40] and adrenals [48] have already been noticed to accumulate efficiently nanoparticles. Other organs in which a significant fluorescent signal is observed are liver and intestine. It has to be noticed that in comparison with other previously described nanovectors, number of which are known to accumulate in high doses in the liver [1,2,49], LNP accumulation in this RES organ is limited. There is no indication of a possible clearance of the fluorescence signal by the kidneys, which is consistent with the 35 nm diameter size of the LNP, larger than the few (1–3) nm of the DiD or Cy5 dyes. There rather exist signs indicative of a hepato-biliary metabolization mechanism, classical for lipids, such as the relatively important fluorescence signal in the intestine. This hypothesis is currently being checked by complementary experiments specially focused on that point. However, it already appears that ligand-functionalized LNP should present all the specifications for achieving *in vivo* specific targeting, all the more than the relatively small size of the particles (35 nm diameter), and therefore their high surface/volume ratio should allow the presentation at their surface of a relatively dense coating of targeting ligands (presumably 50–200 per particle).

4.4. cRGD targeting in HEK293(β3) and TS/A-pc models

In vitro test of cRGD-functionalized LNP in the presence of HEK293(β3) cells validates the functionalization step, as well as the specificity of $\alpha_v\beta_3$ integrin binding and internalization, in comparison with LNP-cRAD and LNP-OH. Once the functionalization of the particles assessed *in vitro*, *in vivo* tests are carried out using two different tumor models – HEK293(β3) and TS/A-pc – implanted subcutaneously in *Nude* mice. Both tumor models express $\alpha_v\beta_3$ integrins on the cell membranes [29–32]. In both cases, significant tumor over skin fluorescence signal is observed a few hours (6–48 h) following intravenous injection of LNP-cRGD (10 nmol of dye, 7.1 mg of total lipids). In the case of HEK293(β3), this fluorescence signal is more pronounced in the presence of LNP-cRGD, in the sense that the same injected doses of LNP-cRAD and LNP-OH lead to lower tumor over skin fluorescence ratio (LNP-cRGD: $T/S = 1.53 \pm 0.07$ ($n = 3$), LNP-OH: $T/S = 1.18 \pm 0.09$ ($n = 3$), LNP-cRAD: $T/S = 1.37 \pm 0.09$ ($n = 3$) 24 h after injection). Concerning the TS/A-pc model, no specificity due to the particle functionalization is observed: tumor over skin fluorescence ratio is similar for LNP-cRGD (2.60 ± 0.48 ($n = 3$)), LNP-cRAD (2.40 ± 0.13 ($n = 3$)), LNP-OH (2.61 ± 0.21 ($n = 3$)). Both cell lines express $\alpha_v\beta_3$ integrins [29–32]; however, the growth of the tumor is very different in the two models. After sub-cutaneous injection in mice, the human HEK293(β3) cells that over-express high levels of integrin are growing slowly (≈6 weeks for reaching 5-mm-diameter tumor), inducing a well-organized and structured neo-angiogenic vessel network for tumor supply [29–31]. On the contrary, TS/A-pc cells grow very fast (≈10 days for reaching 5-mm-diameter tumor) and express low level of $\alpha_v\beta_3$ integrin: the fast-build angiogenic vessels display very leaky fenestrations [32]. In such a tumor model, nanoparticles are known to extravasate very efficiently due to the passive (i.e. non-targeted) EPR effect. This passive extravasation and tumor tissue accumulation of the particles could occur whatever the LNP coating groups and would account for the similar fluorescence over skin ratio obtained for LNP-cRGD, LNP-cRAD, and LNP-OH in the TS/A-pc model. In the HEK293(β3) model, particle passive accumulation due to the EPR effect should be reduced because of the tight endothelial junction of the well-built neo-angiogenic vessels. In addition, a strong captation of RGD-targeted nanoparticles can be obtained by the tumor cells themselves since they express high amounts of the $\alpha_v\beta_3$ integrin. Therefore, no significant EPR effect should occur, and it could become possible to assess a different particle behavior according to their coating. In this case, a slight augmented uptake is observed with LNP-cRGD in comparison with LNP-OH. Surprisingly, a small effect of the cRAD peptide functionalization is observed *in vivo* (Fig. 3), which is far less pronounced *in vitro* on the percentage of LNP-cRAD binding and internalization (Fig. 2). This could be explained by subtle modifications of the surface of the particles after addition of the different peptides, which may favor their bio-availability. These

first results underline the disparity that might exist between different study models, such as the slow-growing tumor model (HEK293(β3)) and the fast-growing tumor model (TS/A-pc). Future work should encompass the validation of functionalized LNP in an even more extended range of biological models, such as for example tumor-induced models.

These results constitute a first proof of concept of LNP vectorization for imaging and drug delivery purposes. Whatever the biological model use, improving targeting efficiency in the future will imply both an optimization of the number of targeted ligands present at the particle interface, and an optimization of their presentation pattern. It has been shown that the number of targeting ligands present on the surface of nanocarriers should be optimized to find out the right balance. *In vitro* targeting efficiency might increase with the density of ligands grafted onto the nanoparticle surface, but screening the POE coating to achieve high ligand density is detrimental for the plasma circulation of the vectors, leading ultimately to poor *in vivo* results [50]. In the present study, long POE_{5000} chains (DSPE-POE_{5000}-maleimide, 9% of the whole POE coating of the particle) have been used to present the cRGD targeting ligands "above" the nanoparticle POE coating (Mirj®53, POE_{2000}), at a moderate ligand density of probably ≈50–200 motifs per particle. It has been demonstrated that the length of the POE chain linking the ligand to the nanoparticles also displays an optimum: if the tethering spacer is too small, but also too long (because of folding), the ligand is embedded in the POE coating and cannot interact efficiently with the cell membrane [51]. Optimization of the ligand density and the length of the POE tethering chain will be carried out in the future, but increasing the number of DSPE-POE-maleimide surfactants or modifying their nature could impact the particle stability, and this point has to be studied carefully. Concerning the presentation of the ligands, it has been shown by our group [29,52–54] and others [25,26,55] that multimeric presentation of the cRGD peptide favors the efficiency of the cRGD/$\alpha_v\beta_3$ integrin recognition and ultimately its internalization in the targeted cell. In particular, the use of a cyclodecapeptide scaffold allowing tetrameric presentation of cRGD [52–54] is expected in the future to improve the LNP targeting efficiency in comparison with the monomeric cRGD ligands used in this study. The results have also stressed out the need to compare active nanoparticle targeting obtained because of the presence of specific ligands, like cRGD, with nanovectors functionalized by reliable negative control, like cRAD, since the simple addition of an organic coating on the surface may strongly affect the behavior of the particles. This observation should therefore be taken into consideration in further studies focused on the optimization of the number and presentation of the ligands onto the LNP surface.

Dye-loaded lipid nanoparticles can be used as *in vivo* imaging agents as themselves, but also constitute a proof-of-principle of the potentialities of cRGD-LNP nanocarriers for vectorizing other imaging agents or therapeutic drugs. Therapeutic applications will require suitable release of the transported active ingredient. Depending on the aimed therapeutic application, prolonged continuous plasma release or specific targeting followed by local release are desired. Study of LNP release profile is beyond the scope of the present work and will be addressed in the future. However, LNP vectorization seems promising for applications requiring an efficient and plasma-stable encapsulation of highly lipophilic loads, such as the DiD dye ($\log P \approx 10$). The preliminary bio-distribution results obtained in this study tend to demonstrate that the very strong lipophily of the DiD dye which is encapsulated within the oily core and not at the particle surface, and the high density of the LNP POE coating which prevents protein binding, should minimize any burst release effect observed for other particles such as liposomes [3], while lipophilic drug-loaded LNP circulate in plasma. However, once cells of interest are targeted (in this case $\alpha_v\beta_3$ integrin over-expressing cells), it might be highly desirable that particle release occurs. LNP release profile and mechanisms will be addressed in the future.

5. Conclusions

In conclusion, new lipid nanoparticles (LNP) responding to the specifications of *in vivo* applications have been designed: they are constituted of ingredients that have been approved by the FDA for human use, have a high colloidal stability, a small size (35 nm diameter), and a neutral POE coating ($\zeta = -5$ mV). They can be functionalized by different peptide ligands, such as cRGD known to specifically bind to $\alpha_v\beta_3$ integrins expressed in neoangiogenic process and at the surface of numerous tumor cell lines [24,25], while keeping their functionality and targeting effect *in vitro* and *in vivo*. Further *in vivo* experiments are necessary to better assess LNP potentialities, especially as drug delivery systems. However, along with an easy to scale-up and very reproducible manufacturing process, based on low cost ingredients, LNP nanovectors present the suitable physico-chemical parameters for realistic and promising *in vivo* applications.

Acknowledgements

This work is supported by the Commissariat à l'Energie Atomique and the French National Research Agency (ANR) through Carnot funding and Contract No. ANR-08-PNANO-006-02. We acknowledge Anne-Claude Couffin (CEA, LETI-DTBS) for helpful remarks and discussion in writing the manuscript.

References

[1] V.P. Torchilin, Multifunctional nanocarriers, Adv. Drug Deliv. Rev. 58 (2006) 1532–1555.
[2] P. Couvreur, C. Vauthier, Nanotechnology: intelligent design to treat complex disease, Pharm. Res. 23 (2006) 1417–1450.
[3] D. Peer, J.M. Karp, S. Hong, O.C. Farokhzad, R. Margalit, R. Langer, Nanocarriers as an emerging platform for cancer therapy, Nat. Nanotechnol. 2 (2007) 751–760.
[4] W. Jiang, B.Y. Kim, J.T. Rutka, W.C. Chan, Advances and challenges of nanotechnology-based drug delivery system, Expert Opin. Drug Deliv. 4 (2007) 621–633.
[5] R.H. Müller, M. Radtke, S.A. Wissing, Nanostructured lipid matrices for improved microencapsulation of drugs, Int. J. Pharm. 242 (2002) 121–128.
[6] R.H. Müller, M. Radtke, S.A. Wissing, Solid lipid nanoparticles (SLN) and nanostructured lipid carriers (NLC) in cosmetic and dermatological preparations, Adv. Drug Deliv. Rev. 54 (2002) S131–S155.
[7] N. Düzgünes, Lipid assemblies for drug delivery, Adv. Drug Deliv. Rev. (2001) 137–138.
[8] V.P. Torchilin, Micellar nanocarriers: pharmaceutical perspectives, Pharm. Res. 24 (2007) 1–15.
[9] J.D. Glickson, S. Lund-Katz, R. Zhou, H.S. Choi, I.W. Chen, H. Li, I. Corbin, A.V. Popov, W. Cao, L. Song, C. Qi, D. Marotta, D.S. Nelson, J. Chen, B. Chance, G. Zheng, Lipoprotein nanoplatform for targeted delivery of diagnostic and therapeutic agents, Mol. Imag. 7 (2008) 101–110.
[10] J.C. Frias, M.J. Lipinski, S.E. Lipinski, M.T. Albeda, Modified lipoproteins as contrast agents for imaging atherosclerosis, Contrast Media Mol. Imag. 2 (2007) 16–23.
[11] V.P. Torchilin, Recent advances with liposomes as pharmaceutical carriers, Nat. Rev. Drug Discov. 4 (2005) 145–160.
[12] S. Heuschkel, A. Goebel, R.H. Neubert, Microemulsions-modern colloidal carrier for dermal and transdermal drug delivery, J. Pharm. Sci. 97 (2008) 603–631.
[13] T.G. Mason, J.N. Wilking, K. Meleson, C.B. Chang, S.M. Graves, Nanoemulsions: formation, structure, and physical properties, J. Phys. Condens. Mater. 18 (2006) R635–R666.
[14] S. Tamilvanan, Oil-in-water lipid emulsions: implications for parenteral and ocular delivering systems (review), Prog. Lipid Res. 43 (2004) 489–533.
[15] W. Mehnert, K. Mäder, Solid lipid nanoparticles: production, characterization and applications, Adv. Drug Deliv. Rev. 47 (2001) 165–196.
[16] H.L. Wong, R. Bendayan, A. Rauth, Y. Li, X.Y. Wu, Chemotherapy with anticancer drugs encapsulated in solid lipid nanoparticles, Adv. Drug Deliv. Rev. 59 (2007) 491–504.
[17] B. Heurtault, P. Saulnier, B. Pech, J.-E. Proust, J.-P. Benoit, A novel phase inversion-based process for the preparation of lipid nanocarriers, Pharm. Res. 19 (2002) 875–880.

[18] S. Liu, S. Wang, R. Lu, Lipoproteins as pharmaceutical carriers, in: V.P. Torchilin (Ed.), Nanoparticles as Drug Carriers, Imperial Press College, 2006.
[19] B. Heurtault, P. Saulnier, B. Pech, J.-E. Proust, J.-P. Benoit, Physico-chemical stability of colloidal lipid particles, Biomaterials 24 (2003) 4283–4300.
[20] I. Texier, M. Goutayer, A. Da Silva, L. Guyon, N. Djaker, V. Josserand, E. Neumann, J. Bibette, F. Vinet, Cyanine loaded lipid nanoparticles for improved in vivo fluorescence imaging, J. Biomed. Opt. 14 (2009) 054005.
[21] T.F. Massoud, S.S. Gambhir, Molecular imaging in living subjects: seeing fundamental biological processes in a new light, Genes Dev. 17 (2003) 545–580.
[22] J. Rao, A. Dragulescu-Andrasi, H. Yao, Fluorescence imaging in vivo: recent advances, Curr. Opin. Biotechnol. 18 (2007) 17–25.
[23] M. Rudin, M. Rausch, M. Stoeckli, Molecular imaging in drug discovery and development: potential and limitations of nonnuclear methods, Mol. Imag. Biol. 7 (2005) 5–13.
[24] M. Schottelius, B. Laufer, H. Kessler, H.-J. Wester, Ligands for mapping $\alpha_v\beta_3$-integrin expression in vivo, Acc. Chem. Res. 42 (2009) 969–980.
[25] A.J. Beer, M. Schwaiger, Imaging of integrin $\alpha_v\beta_3$ expression, Cancer Metast. Rev. 27 (2008) 631–644.
[26] K. Temming, R.M. Schiffelers, G. Molema, R. Kok, RGD-based strategies for selective delivery of therapeutics and imaging agents to the tumor vasculature, Drug Resist. Updates 8 (2005) 381–402.
[27] R. Haubner, R. Gratias, B. Diefenbach, S. Goodman, A. Jonczyk, H. Kessler, Structural and functional aspects of RGD-containing cyclic pentapeptides as highly potent and selective integrin avb3 antagonists, J. Am. Chem. Soc. 118 (1996) 7461–7472.
[28] R. Haubner, D. Finsinger, H. Kessler, Stereoisomeric peptide libraries and peptidomimetics for designing selective inhibitors of the $\alpha_v\beta_3$ integrin for a new cancer therapy, Angew. Chem. Int. Ed. 36 (1997) 1374–1389.
[29] Z.H. Jin, V. Josserand, S. Foillard, D. Boturyn, P. Dumy, M.C. Favrot, J.L. Coll, In vivo optical imaging of integrin alpha(v)-beta(3) in mice using multivalent or monovalent cRGD targeting vectors, Mol. Cancer 6 (2007), doi:10.1186/1476-4598-6-41.
[30] Z.-H. Jin, J. Razkin, V. Josserand, D. Boturyn, A. Grichine, I. Texier, M. Favrot, P. Dumy, J.L. Coll, In vivo noninvasive optical imaging of receptor-mediated RGD internalization using self-quenched Cy5-labeled RAFT-c-(-RGDfK-)4, Mol. Imag. 6 (2007) 43–55.
[31] J. Razkin, V. Josserand, D. Boturyn, Z. Jin, P. Dumy, M. Favrot, J.L. Coll, I. Texier, Activatable fluorescent probes for tumor-targeting imaging in live mice, ChemMedChem 1 (2006) 1069–1072.
[32] L. Sancey, V. Ardisson, L.M. Riou, M. Ahmadi, D. Marti-Batlle, D. Boturyn, P. Dumy, D. Fagret, C. Ghezzi, J.P. Vuillez, In vivo imaging of tumour angiogenesis in mice with the alpha(v)beta(3) integrin-targeted tracer Tc-99m-RAFT-RGD, Eur. J. Nucl. Med. Mol. Imag. 34 (2007) 2037–2047.
[33] R. Sens, K.H. Drexhage, Fluorescence quantum yield of oxazine and carbazine laser dyes, J. Lumin. 24–25 (1981) 709–712.
[34] Z.H. Jin, V. Josserand, J. Razkin, E. Garanger, D. Boturyn, M.C. Favrot, P. Dumy, J.L. Coll, Noninvasive optical imaging of ovarian metastases using Cy5-labeled RAFT-c(-RGDfK-)(4), Mol. Imag. 5 (2006) 188–197.
[35] I. Texier, V. Josserand, E. Garanger, J. Razkin, Z. Jin, P. Dumy, M. Favrot, D. Boturyn, J.-L. Coll, Luminescent probes for optical in vivo imaging, Proc. SPIE 5704 (2005) 16–23.
[36] M. Ferrari, Cancer nanotechnology: opportunities and challenges, Nat. Rev. Cancer 5 (2005) 161–171.
[37] H. Maeda, J. Wu, T. Sawa, Y. Matsumura, K. Hori, Tumor vascular permeability and the EPR effect in macromolecular therapeutics: a review, J. Control. Release 65 (2000) 271–284.
[38] P. Carmeliet, R.K. Jain, Angiogenesis in cancer and other diseases, Nature 407 (2000) 249–257.
[39] P. Decuzzi, R. Pasqualini, W. Arap, M. Ferrari, Intravascular delivery of nanoparticulate systems: does geometry really matter?, Pharm Res. (2008), doi:10.1007/s11095-008-9697-x.
[40] A.-C. Faure, S. Dufort, V. Josserand, P. Perriat, J.L. Coll, S. Roux, O. Tillement, Control of the in vivo biodistribution of hybrid nanoparticles with different poly(ethyleneglycol) coatings, Small 5 (2009) 2565–2575.
[41] M. Hamidi, A. Azadi, P. Rafiei, Pharmacokinetic consequences of pegylation, Drug Deliv. 13 (2006) 399–409.
[42] S.M. Moghimi, A.C. Hunter, J.C. Murray, Long-circulating and target-specific nanoparticles: theory to practice, Pharmacol. Rev. 53 (2001) 283–318.
[43] C. Monfardini, F.M. Veronese, Stabilization of substances in circulation, Bioconjug. Chem. 9 (1998) 418–450.
[44] N. Anton, J.P. Benoit, P. Saulnier, Design and production of nanoparticles formulated from nano-emulsion templates – a review, J. Control. Release 128 (2008) 185–194.
[45] S. Sajjadi, Nanoemulsion formation by phase inversion emulsification: on the nature of inversion, Langmuir 22 (2006) 5597–5603.
[46] L. Wang, X. Li, G. Zhang, J. Dong, J. Eastoe, Oil-in-water nanoemulsions for pesticide formulations, J. Colloid Interf. Sci. 314 (2007) 230–235.
[47] S.M. Jafari, Y.H. He, B. Bhandari, Nano-emulsion production by sonication and microfluidization – a comparison, Int. J. Food Prop. 9 (2006) 475–485.
[48] R. Weissleder, Y.M. Wang, M. Papisov, A. Bogdanov, B. Schaffer, T.J. Brady, J. Wittenberg, Polymeric contrast agents for MR imaging of adrenal glands, JMRI – J. Magn. Reson. Imag. 3 (1993) 93–97.
[49] T.J. Daou, L. Li, P. Reiss, V. Josserand, I. Texier, Effect of poly(ethylene glycol) length on the in vivo behavior of coated quantum dots, Langmuir 25 (2009) 3040–3044.
[50] K.M. McNeeley, A. Annapragada, R.V. Bellamkonda, Decreased circulation time offsets increased efficacy of PEGylated nanocarriers targeting folate receptors of glioma, Nanotechnology 18 (2007) 385101.
[51] R.R. Sawant, R.M. Sawant, A.A. Kale, V.P. Torchilin, The architecture of ligand attachment to nanocarriers controls their specific interaction with target cells, J. Drug Target. 16 (2008) 596–600.
[52] D. Boturyn, J.L. Coll, E. Garanger, M. Favrot, P. Dumy, Template assembled cyclopeptides as multimeric system for integrin targeting and endocytosis, J. Am. Chem. Soc. 126 (2004) 5730–5739.
[53] E. Garanger, D. Boturyn, J.L. Coll, M. Favrot, P. Dumy, Multivalent RGD synthetic peptides as potent $\alpha_v\beta_3$ integrin ligands, Org. Biomol. Chem. 4 (2006) 1958–1965.
[54] E. Garanger, D. Boturyn, Z. Jin, P. Dumy, M. Favrot, J.L. Coll, New multifunctional molecular conjugate vector for targeting, imaging and therapy of tumors, Mol. Ther. 12 (2005) 1168–1175.
[55] Z. Cheng, Y. Wu, Z. Xiong, S.S. Gambhir, X. Chen, Near-infrared fluorescent RGD peptides for optical imaging of integrin $\alpha_v\beta_3$ expression in living mice, Bioconjug. Chem. 16 (2005) 1433–1441.